A Freshwater Starvation Mechanism for Dansgaard-Oeschger Cycles

Hewitt, I.J. and Wolff, E.W. and Fowler, A.C. and Clark, C.D and Evatt, G.W. and Munday, D.R. and Stokes, C.R.

2015

MIMS EPrint: **2015.35**

Manchester Institute for Mathematical Sciences
School of Mathematics

The University of Manchester

Reports available from: http://eprints.maths.manchester.ac.uk/
And by contacting: The MIMS Secretary
School of Mathematics
The University of Manchester
Manchester, M13 9PL, UK

ISSN 1749-9097

A Freshwater Starvation Mechanism for Dansgaard-Oeschger Cycles

I. J. Hewitt[1], E. W. Wolff[2], A. C. Fowler[1,3], C. D. Clark[4], G. W. Evatt[5], D. R. Munday[6], and C. R. Stokes[7]

Ice core records indicate that the northern hemisphere underwent a series of cyclic climate changes during the last glacial period known as Dansgaard-Oeschger cycles. The most distinctive feature of these is a rapid warming event, often attributed to a sudden change in the strength of the Atlantic meridional overturning circulation (AMOC). We suggest that such a change may have occurred as part of a natural oscillation, which resulted from salinity changes driven by the temperature-controlled runoff from ice sheets. Contrary to many previous studies, this mechanism does not require large freshwater pulses to the North Atlantic. Instead, steady changes in ice-sheet runoff, driven by the AMOC, lead to a naturally arising oscillator, in which the rapid warmings come about because the Arctic Ocean is starved of freshwater. The changing size of the ice sheets, as well as changes in the background climate, would have affected the magnitude and extent of runoff, which altered the period and magnitude of individual cycles. We suggest that this may provide a simple explanation for the absence of the events during interglacials and around the time of glacial maxima.

1. Introduction

Many northern hemisphere climate records, particularly those from around the North Atlantic, show a series of rapid climate changes that recurred on centennial to millennial timescales throughout most of the last glacial period [*Dansgaard et al.*, 1993; *Wolff et al.*, 2010]. Figure 1 shows a segment of an ice core record from Greenland, where the oxygen isotope signal represents a proxy measurement of temperature, and time progresses from right to left. The record shows a whole sequence of distinctive events, most notably recognised by the sudden warming, indicated by a rapid rise of the δ^{18}O signal. This sharp rise is followed by a slower cooling, and then in most cases, by a more abrupt cooling.

These Dansgaard-Oeschger (D-O) sequences are observed most prominently in Greenland ice cores [*Johnsen et al.*, 1992; *North Greenland Ice Core Project Members*, 2004]. The warming jumps are of order 10°C, and typically occur in 40 years, while the slow cooling (Greenland Interstadial, GI) lasts between a few centuries and a few millennia; the eventual rapid temperature drop starts a cold Greenland Stadial (GS) that lasts for a similar period [*Wolff et al.*, 2010]. D-O events occur throughout the last glacial period, though they are rare during the very coldest glacial periods (Marine isotope stages 2 and 4), and nothing of similar magnitude occurs during the current interglacial. Although there are no Greenland ice cores extending into earlier glacial cycles, there is good evidence that they are ubiquitous in the glacial periods of the last 800,000 years [*Jouzel et al.*, 2007]. Temperature excursions that match those seen in Greenland, though with reduced amplitude, are observed around the North Atlantic [*Shackleton et al.*, 2000], and climate signals with the same pattern are observed in other palaeoclimate proxies throughout the northern hemisphere [*Wang et al.*, 2001; *Peterson et al.*, 2000].

Soon after their existence was confirmed, it was suggested that D-O events were caused by variations in the strength or style of the Atlantic Meridional Overturning Circulation (AMOC), driven either by discrete flood events [*Broecker et al.*, 1988], or by natural salinity oscillations [*Broecker et al.*, 1990; *Birchfield and Broecker*, 1990]. Numerous studies since then have assumed that D-O events are principally driven by changes in the AMOC but, probably because of the discovery at about the same time of Heinrich events (evidence for the input of freshwater through large iceberg events) [*Heinrich*, 1988; *Bond et al.*, 1992; *Hemming*, 2004], most discussion has centred on pulses of freshwater as drivers of AMOC weakening (e. g., *Rahmstorf* [1995]; *Clark et al.* [2001]). One recent paper [*Zhang et al.*, 2014] suggested that the AMOC changes might have been promoted by variations in the Laurentide ice sheet that caused subtle changes in atmospheric circulation and sea ice. However little recent work has returned to the simple idea of natural cycles in salinity, or has explained the apparently self-sustaining nature of the observed cycles, although such ideas are still promoted [*Wang and Mysak*, 2006; *Peltier and Vettoretti*, 2014].

A contrasting pattern to the northern hemisphere cycles is seen in some southern hemisphere records, particularly those from Antarctic ice cores: while Greenland experiences the cold stadial, Antarctica slowly warms, and while Greenland is in its warmer interstadial state, Antarctica slowly cools [*Blunier and Brook*, 2001; *EPICA Community Members*, 2006]. The contrasting interhemispheric signal matches in quite some detail that expected from a simple model for a bipolar seesaw mechanism [*Stocker and*

[1]Mathematical Institute, University of Oxford, OX2 6GG, UK
[2]Department of Earth Sciences, University of Cambridge, UK
[3]MACSI, University of Limerick, Ireland
[4]Department of Geography, University of Sheffield, S10 2TN, UK
[5]Department of Mathematics, University of Manchester, UK
[6]British Antarctic Survey, UK
[7]Department of Geography, Durham University, DH1 3LE, UK

0883-8305/15/$12.00

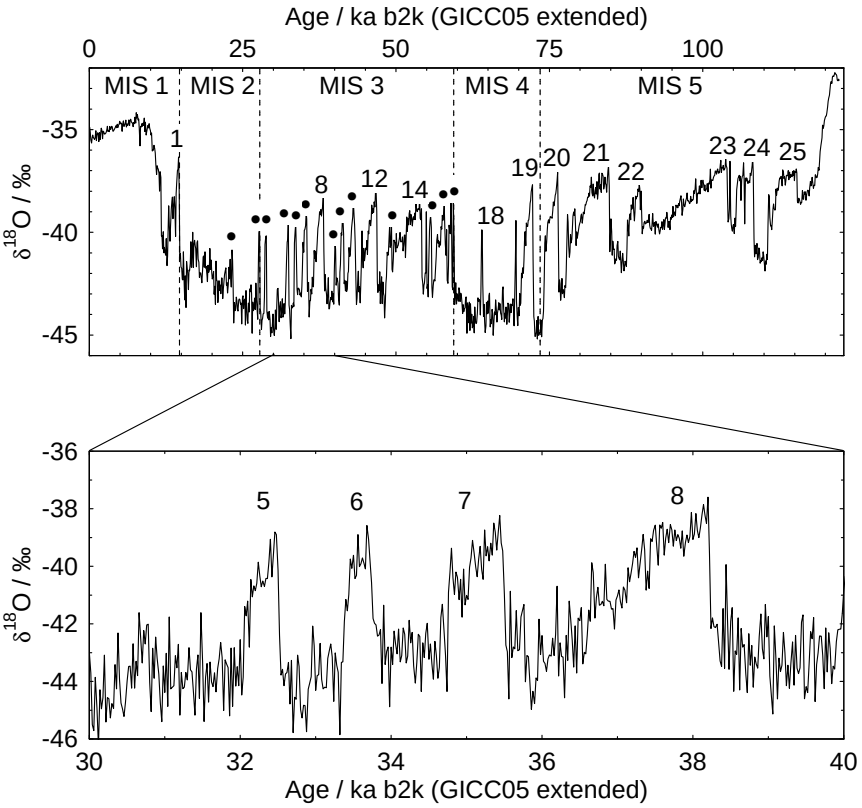

Figure 1. Oxygen isotope data from the NorthGRIP ice core in Greenland as a function of age in thousands of years. The different marine isotope stages are numbered, as are 25 Dansgaard–Oeschger events. The lower panel shows an enlarged view of the period 30-40 ka.

Johnsen, 2003; *Barker et al.*, 2011]. This adds support to the idea that changes in the AMOC are an inherent aspect of D-O cycles.

The simplest explanation that associates AMOC variability with rapid climate change relates to Stommel's concept of hysteresis in the ocean circulation [*Stommel*, 1961], whereby a suitable forcing can cause a switch between strong and weak circulation, the stronger state being associated with a warmer Northern hemisphere climate. The most common such forcing applied in models is the so-called 'hosing' of the North Atlantic, in which a supply of freshwater is prescribed [eg. *Kageyama et al.*, 2013].

Some mechanisms have been advanced that do not involve AMOC changes as their main component. In particular a number of proposals are centred on rapid changes in the winter sea ice edge [*Gildor and Tziperman*, 2003; *Li et al.*, 2005], most recently with the addition of a role for an ice shelf whose growth timescale paces the cycles [*Petersen et al.*, 2013]. Although increases in sea ice latitudinal extent will undoubtedly push the circulation system southwards, it is not clear that sea ice mechanisms without AMOC changes would produce the observed bipolar seesaw pattern of change. Several proposed mechanisms incorporate both sea ice change and changes in ocean circulation [*Denton et al.*, 2005; *Dokken et al.*, 2013]. In this paper we focus on the AMOC change, but we recognise that a strong response of sea ice is likely to be a very important amplifier of temperature change in the north.

Many of the climate signals observed worldwide could be explained by a varying AMOC strength driven by variations in freshwater input [*Menviel et al.*, 2014]. What has never been fully explained is how and why such variable hosing should occur. Since Dansgaard–Oeschger events are associated with the presence of ice sheets, the most obvious freshwater source consists of the ice sheets themselves, and most simply, a variable supply may be a consequence of a variable rate of meltwater generation as the ice sheet expands and contracts [*Clark et al.*, 2001]. Indeed, freshwater input variations of the order of 0.1 Sv = 10^5 m^3 s^{-1} are found necessary in models to fuel the AMOC fluctuations [*Ganopolski and Rahmstorf*, 2001], and such a flux is comparable to deglaciation net runoff rates (120 m sea level rise in 10,000 years constitutes an average flux of 0.14 Sv), which indicates that this provides a reasonable freshwater source. More generally, the variable freshwater input is assumed to involve some combination of water and icebergs from the Laurentide Ice Sheet [*Carlson and Clark*, 2012].

While a variable melt supply seems to provide a reasonable source, the mechanism that would produce such variability in a semi-regular fashion remains obscure. The paper of *Ganopolski and Rahmstorf* [2001] is a good illustration of this: their model of intermediate complexity convincingly produces Dansgaard–Oeschger events given a prescribed sinusoidally fluctuating freshwater source of total variation

0.06 Sv. As *Petersen et al.* [2013] comment, "there is no known physical mechanism to explain such a sinusoidal fluctuation". Our purpose in this paper is to show that when the mechanics of melt supply are included, such oscillations can arise naturally.

The ideas of the present paper are complementary to those of *Peltier and Vettoretti* [2014]. Peltier and Vettoretti present numerical results from a sophisticated computational model of coupled ocean-atmosphere dynamics, in which it is shown that almost periodic oscillations in AMOC can occur in a glacial climate (in which the reconstructed ice sheets remain stationary). As here, they find that the oscillations are due to salinity variations in the North Atlantic, associated with a gradual variation in sea ice response. As we discuss later, the mechanics of this oscillation are not dissimilar to our much simpler model. A similar study was made by *Wang and Mysak* [2006], who found self-sustained oscillations in AMOC in a model of intermediate complexity. In addition, they studied the variability of D-O events as the climate cools. Their discussion resembles some of that we give below, although our simpler model will allow a more specific interpretation of the variability. Our explanation also represents an elaboration of the ideas of *Broecker et al.* [1990], *Birchfield and Broecker* [1990] and *Clark et al.* [2001]. Indeed our model eventually (but not initially) resembles that of *Birchfield and Broecker* [1990], and we comment further on this in the discussion.

We suggest that air temperature and consequently meltwater runoff from the northern hemisphere ice sheets varied significantly with the strength of the AMOC, and that the resulting variation in effective freshwater delivery to the North Atlantic induces a natural self-sustained oscillation that provides a simple explanation for the D-O sequences. It also provides a potential explanation for varying occurrence and period of D-O events as a function of ice sheet size and background climate.

2. A simple model

Numerical models of ocean circulation suggest that multiple equilibrium states of AMOC are possible, and that as freshwater delivery to the North Atlantic varies, sudden switches can occur [eg. *Ganopolski and Rahmstorf*, 2001; *Rahmstorf et al.*, 2005; *Hawkins et al.*, 2011]. Simplified models, building on the original work of *Stommel* [1961] find similar hysteretic behaviour [*Johnson et al.*, 2007]. This behaviour is shown schematically in figure 2, and in our simple discussion, we take this result as given.

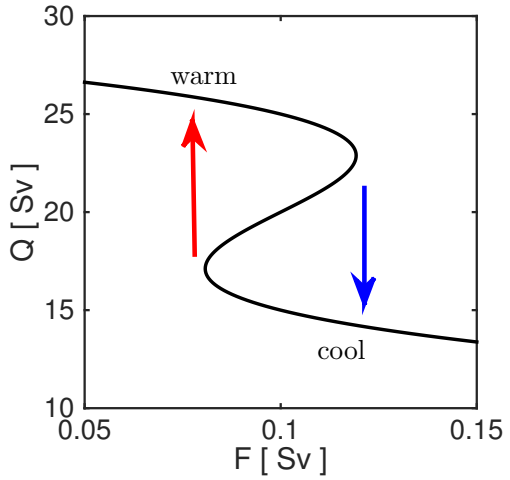

Figure 2. Typical pattern of AMOC strength Q found in ocean models, depending on North Atlantic freshwater flux F. In our simple model, this curve is described by the function $F = F_0 + \Phi(Q)$.

It has recently been suggested [*Condron and Winsor*, 2012] that only meltwater discharged via the Mackenzie River route into the Arctic Ocean leads to a significant weakening of Labrador and Greenland Sea convection, and hence to a large reduction in AMOC and northward heat transport. While Condron and Winsor considered the effect of a large instantaneous release of meltwater, a simple reduction or enhancement of runoff will slowly change mean Arctic salinity, and hence change the effective freshwater supply to the North Atlantic through the Fram Strait (and Canadian Arctic Archipelago, if open). Thus, a strong AMOC leads, through warmer temperatures, to greater runoff into the Arctic. This causes a gradual freshening until the salinity of the water entering the North Atlantic is low enough to switch the AMOC into a weaker state. Now, the colder temperatures over the ice sheet mean that the Arctic is starved of freshwater, its salinity rises, eventually causing the AMOC to strengthen again.

We will show, using a simple dynamical model, that this natural cyclic behaviour, inherent to the system, provides a simple explanation for the D-O cycles. Changes in the routing and sensitivity of the meltwater runoff, depending on ice sheet size, provide a possible explanation for the variability which is seen in the ice core record.

The overturning circulation strength Q depends on the freshwater flux F to the North Atlantic, as in figure 2, with two different stable equilibrium strengths for some values of F (the definition of F is made more explicit below). This can be described mathematically by supposing that, in equilibrium, F is a prescribed non-monotonic function $f(Q)$ of the overturning circulation Q. To be specific, and as in figure 2, we take the function $f(Q)$ to be a simple cubic, centred about the point (F_0, Q_0):

$$f(Q) = F_0 + \Phi(Q), \tag{1}$$

where

$$\Phi(Q) = b(Q - Q_0)\left\{1 - \left(\frac{Q - Q_0}{\Delta Q}\right)^2\right\}, \tag{2}$$

and the values of b, Q_0 and ΔQ are chosen to be

$$b = 0.01, \quad Q_0 = 20 \text{ Sv}, \quad \Delta Q = 5 \text{ Sv}, \tag{3}$$

(both F and Q are measured in s Sverdrups, 1 Sv $= 10^6$ m^3 s^{-1}). These values are chosen to give a sensitivity between Q and F comparable to that shown in the model results of *Ganopolski and Rahmstorf* [2001] (their figure 1) for glacial climates. The precise values and form of the function $\Phi(Q)$ are not important.

Other things being equal, for a given value of F, the circulation Q will approach equilibrium on either the upper or lower branch of the curve (the middle branch, as usual in such hysteretic curves, is unstable), and a very simple way to represent this is to take the dynamics of Q to be governed by the first order differential equation

$$b\tau\frac{dQ}{dt} = f(Q) - F. \tag{4}$$

Here τ is a time scale which is representative of the rate at which Q approaches equilibrium (this is because, for $Q \sim Q_0$, $f'(Q) \sim b$).

The mechanism of the oscillations found by *Ganopolski and Rahmstorf* [2001] is then simply explained in terms of figure 2. A prescribed slowly varying (on a time scale much longer than τ) freshwater flux F will in turn reach the edge of the warm and cool branches, at which point there is a rapid transition to the other branch, as indicated by the red and blue arrows. The red arrow indicates a sudden warming, and the blue arrow a sudden cooling, and this sequence of transitions can very simply reproduce the general shape of the D-O events shown in figure 1. As before, the question arises as to what can cause the fluctuations of F. In particular, the long duration ($\sim$ 1000 years in figure 1) is associated with the slow changes in F, while the rapid decadal warming relates to the time scale τ.

We now wish to incorporate the effect suggested by *Clark et al.* [2001], namely that varying meltwater runoff to the North Atlantic can occur in association with fluctuations of the ice margin. There are a number of inter-related considerations here. Most simply, and this is our assumption, the runoff R will depend directly on temperature, which itself depends directly on oceanic circulation Q. To be specific, we assume a linear dependence of R on AMOC via its assumed dependence on temperature T:

$$R = R_0 + \lambda\,(Q - Q_0)\,; \tag{5}$$

R_0 is a suitable reference value, and λ is a positive constant. It is quite likely that this relationship is amplified by large changes in the sea ice edge [*Li et al.*, 2005], which are needed to explain the magnitude of observed climate change in Greenland; however for the simple formulation of this paper, the sea ice changes are absorbed into the response of R to Q. A complicating effect is that on a slower time scale, the ice margin will retreat in warm periods, and this will have a buffering effect of reducing the ice available to melt; however, while margin position will certainly affect runoff, it seems reasonable to suppose that the margin responds to warming on a much longer time scale than that associated with the individual events, so that in the first instance we do not consider this effect further; see also the discussion section.

A second complication arises due to the fact that advance and retreat of the Laurentide Ice Sheet causes re-routing of the drainage pathways [*Clark et al.*, 2001], and this may have a profound effect on our model description; again, the time scales should be long and the switching can be ignored in terms of the dynamics of individual events, although it is likely to be important in terms of long term variability in D-O event occurrence.

Implicit in (5) is that the drainage is steady. Although there is plenty of evidence that drainage from proglacial lakes [*Bretz*, 1923; *Clarke et al.*, 2004] and subglacial lakes [*Wingham et al.*, 2006; *Fricker and Scambos*, 2009] can be unsteady in time, and this may have some bearing on the variability of D-O events, we do not consider the unsteadiness essential to the mechanism and, as such, do not account for it in this analysis.

Before going further into the details of meltwater routing through the Arctic Ocean, it is worth considering what would happen if the runoff R were delivered directly to the North Atlantic, for example along the St. Lawrence valley. In that case we could simply equate the runoff R with the freshwater flux F that drives ocean circulation. The equilibria of (5) would be determined by the (possibly multiple) solutions of $F = f(Q)$ and $F = R(Q)$, and Q will relax to one of these equilibria on a rapid decadal time scale. While the positions of the equilibria might change due to longer-term changes (in ice-sheet extent, for example), and such changes might result in the loss of an equilibrium on one or other of the branches, there are no inherent D-O like oscillations.

As discussed above, there are a number of modifications one might make to this simple model, but the one we illustrate here is possibly the simplest, and takes account of the fact that if meltwater is routed northwards by means of the MacKenzie River, then the intervening Arctic Ocean acts as a buffer in the delivery of the freshwater flux to the North Atlantic, where it controls the AMOC. This can lead to a naturally-occurring relaxation oscillation.

The situation we have in mind is illustrated in figure 3, which is a simplified cartoon in the spirit of the box models of *Stommel* [1961] and *Johnson et al.* [2007]. Fresh water runs off both to the Arctic and North Atlantic, and R is split between a North Atlantic component R_N and an Arctic component R_A:

$$R = R_N + R_A; \tag{6}$$

these are balanced by net evaporative loss E in the North Atlantic and other evaporative loss elsewhere. We assume that Arctic runoff varies with AMOC by analogy with (5):

$$R_A = R_0 + \lambda\,(Q - Q_0)\,; \tag{7}$$

R_N would have a similar dependence, but we ignore this, on the basis of *Condron and Winsor* [2012]'s assertion that it is the Arctic runoff which is important in determining Q.

We suppose the volume and salinity of the North Atlantic are V_N and S_N, respectively, and those of the Arctic are V and S. We assume the ocean volumes remain constant, so that there is a net outflow from the Arctic equal to R_A, which is in addition to an exchange flow X, largely through the Fram Strait. Additionally there is a net outflow of $R_A + R_N - E$ from the North Atlantic to the south.

The question now arises, what is the effective freshwater flux for this system? This is a slightly awkward question, because the freshwater delivered to the Arctic is buffered before its delivery to the North Atlantic. The details are discussed in appendix A, where it is shown that the effective freshwater flux to the North Atlantic can be written as

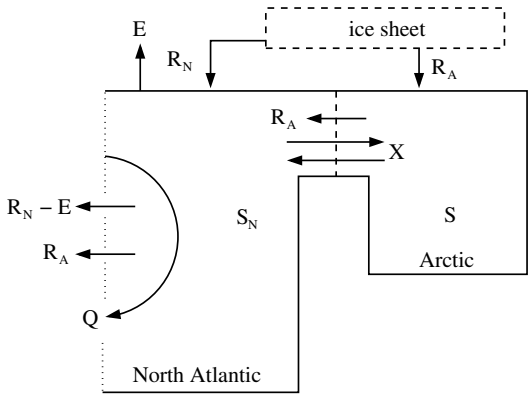

Figure 3. Schematic of the model. Q is the AMOC strength, and is an exchange flow from the North to the South Atlantic; it varies due to an effective freshwater delivery to the North Atlantic F, and it controls northern hemisphere temperature T. The freshwater flux F is driven by Arctic runoff R_A and is buffered by mean Arctic salinity S. R_N denotes alternative meltwater runoff routes direct to the North Atlantic, and E denotes North Atlantic evaporation. Ocean volume is conserved, which results in a compensating flow $R_A + R_N - E$ to lower latitudes.

$F = F_0 + \Delta F$, with

$$\Delta F = \{X + R_0 + \lambda(Q - Q_0)\}\frac{(S_N - S)}{S_N} - R_0 + F_*, \quad (8)$$

where

$$F_* = R_0 + R_N - E - F_0. \quad (9)$$

It is also shown that the Arctic salinity S satisfies the equation (from (A3) and (A6)),

$$V\frac{dS}{dt} = S_N\{\Delta F - F_* - \lambda(Q - Q_0)\}, \quad (10)$$

and the AMOC equation (4) is then

$$b\tau\frac{dQ}{dt} = \Phi(Q) - \Delta F. \quad (11)$$

Equations (10) and (11) describe a two-dimensional dynamical system for the AMOC strength Q and the Arctic salinity S, where the function $\Delta F(Q, S)$ is given by (8), and $\Phi(Q)$ by (2). Before discussing the solutions, we estimate reasonable sizes for the parameters.

It is convenient to suppose that R_N and E are constant during a D-O event (or to consign their variation to Φ). Their precise values are in fact not important, since, by assumption, the base level freshwater flux F_0 must be such that the hysteresis loop comes into play. This suggests that F_* must be relatively small, and thus $F_0 \sim R_0 + R_N - E$, whatever the values of these latter parameters. However, changes of R_N and E, due to slow changes in the background climate and precipitation patterns, can lead to changes in F_* which we later explore. A typical value of runoff during deglaciation is ~ 0.1 Sv [*Tarasov and Peltier*, 2005], and we take this value for the reference-level runoff R_0.

The other parameters to be chosen are the values of V, S_N, λ, X and τ. The value of τ should mimic the fast reaction time of the AMOC, and we choose $\tau = 10$ y. The Arctic Ocean volume is $V = 1.9 \times 10^7$ km^3 [*Eakins and Sharman*, 2010], and the North Atlantic salinity is taken as $S_N = 36$ ppt (although S_N will vary somewhat during the cycles, the variation will be small, so we take it as constant).

It remains to choose X and λ. The present day flow through the Fram Strait has been measured by *Fahrbach et al.* [2001]. They estimate an exchange flow of around 10 Sv, but comment that this is much higher than previous estimates. The flow fluctuates dramatically through the year, and it is likely that the glacial value may have been quite different. In fact, the term X in our model should not be directly equated with the exchange flow through the Fram Strait itself, but rather represents the mixing effect of this flow on the whole Arctic basin. A more consistent method to estimate an appropriate value is to use the approximate balance of the terms on the right hand side of (10), supposing that the present-day situation is close to a steady state. This suggests that $X(S_N - S) \sim R_A S$ and hence $X \sim R_A S/(S_N - S)$. *Aagard and Carmack* [1989] suggest that the net freshwater outflow from the Arctic is ~ 0.1 Sv, and if we use $R_A \sim 0.1$ Sv, $S_N \sim 36$ ppt and $S \sim 34.5$–35 ppt, we find $X \sim 2.3$–3.5 Sv. This suggests a current value around 3 Sv, but we recognise that we might expect lower values in a glacial climate.

To estimate λ, we use a roundabout route. We know that temperature variations in Greenland are ~ 10 K, for a presumed variation of Q of order $2\Delta Q \sim 10$ Sv, and we know that net deglaciation runoff rates are ~ 0.14 Sv. A plausible estimate of the change in melt rate and thus runoff due to a change in summer temperature from say 10° C to 20° is therefore $\Delta R_A \sim 0.1$ Sv, which would correspond to a value of $\lambda \sim \Delta R_A/2\Delta Q \sim 0.01$. We use this as a guiding figure in our simulations. A similar figure can be arrived at by estimating the area of the ice sheets undergoing melting, and the change in ablation rate due to the presumed increase in temperature. Note also that this suggests a relation for temperature change of the form

$$T = T_0 + \alpha(Q - Q_0), \quad (12)$$

with $\alpha \sim 1$ K Sv^{-1}; we also show this temperature sensitivity in figure 4.

Depending on conditions, the simple system described by (10) and (11) can exhibit stable steady states or periodic or-

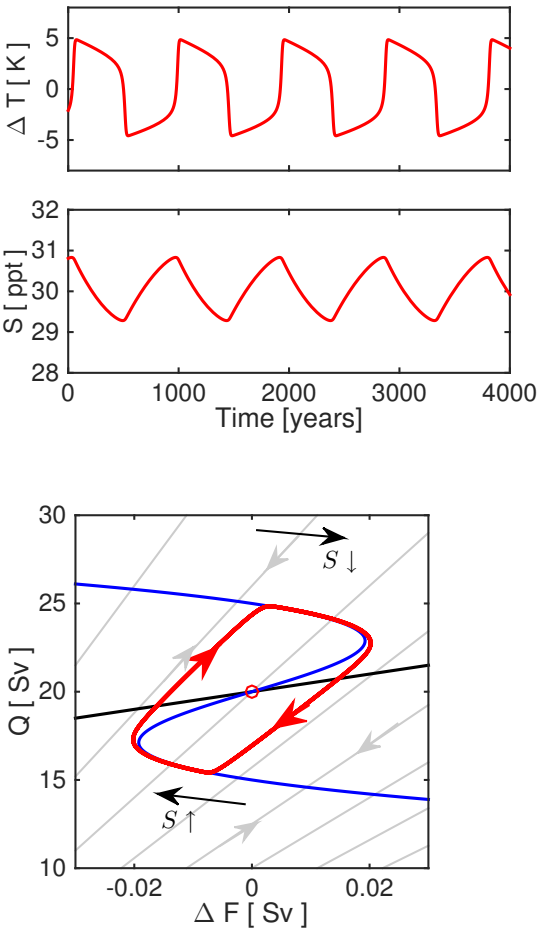

Figure 4. Modelled cycles in Arctic salinity S and northern hemisphere temperature fluctuation ΔT. Parameter values as given in the text, with $F_* = 0$, except that $\lambda = 0.02$ and $X = 0.5$ Sv. The lowest panel shows the path taken on the ΔF–Q phase plane, where ΔF is the change in freshwater flux from its reference value F_0. The red line shows the AMOC nullcline curve $\Delta F = \Phi(Q)$ from (11); to the left of this line Q is always increasing, to the right of it Q is decreasing, and since the change of Q according to (11) is rapid it moves approximately along the grey lines, $\Delta F = \Delta F(Q, S)$ given by (8), on which S is constant. The black line shows the salinity nullcline $\Delta F = F_* + \lambda(Q - Q_0)$; S is always increasing beneath this line and decreasing above it, as shown by the black arrows. The circle marks the (unstable) steady state of the system.

bits in the form of a relaxation oscillator. It is the latter we associate with the D-O cycles. A typical solution is shown in figure 4; while on the upper warm branch of the ocean curve, the Arctic is freshening and the effective freshwater flux increases until it is sufficient to cause a reduction in AMOC and consequent cooling. While on the lower cooler branch, the reduced runoff causes the Arctic to become more saline and eventually leads to rapid strengthening of the AMOC and the sudden warming.

Whether or not the system exhibits the oscillations depends on the shape and intersections of the equilibrium curves for (10) and (11), seen in the lower panel of figure 4. It is also possible to choose parameters that do not give rise to cyclical behaviour, or produce cycles with different properties, and a discussion of these effects is explored in the following section.

3. Discussion

Self-sustained oscillations and parameter dependence

While this model provides a mechanism for self-sustained oscillations, they do not always occur, and the reasons for this can be understood in terms of variants of the phase portrait in figure 4. In that figure, cycles occur when the steady state (the red circle marking the intersection of the two nullclines) lies on the intermediate branch of the hysteresis curve, and if the black nullcline has slope less than the multi-valued blue one at that point. The detailed parameter conditions under which this occurs are analysed in appendix B. However, they can be easily seen by considering the possible changes to the slope and intercept of the black null cline, given from (10) by $\Delta F = F_* + \lambda(Q - Q_0)$. Such changes are shown in figures 5-8.

Varying λ changes the slope; if λ is too small, as in figure 5, there are stable steady states on the upper and lower branches of the AMOC hysteresis curve. In this case, the evolution of Arctic salinity simply causes the system to approach one of these states, and there are no self-sustaining oscillations. It is evident that slow variation of λ above and below a critical value can cause the oscillations to switch on and off in this manner, and this provides a potential explanation for the variability in the recurrence period of the cycles. Indeed, even while the system remains unstable as in figure 4, slow variations in λ cause variations in the period of the cycles and the amplitude of the temperature jumps. As discussed below, such changes in λ might come about because of changes in the background climate, or changes in the size of the ice sheets (recall that λ measures the sensitivity of runoff, via temperature, to strength of the AMOC).

If λ is much larger than necessary to ensure a single steady state, as in figure 6, it is also possible that this steady state becomes stable. This would occur if the slope of the grey lines, which mark the possible paths along which the solution rapidly jumps towards the blue AMOC curve, are themselves less steep than the slope of that nullcline. In appendix B we find that the criterion for this to occur is approximately that $X \lesssim R_0$, and it thus requires almost complete collapse of the Fram Strait exchange flux. We do not think this is normally very likely to occur.

Both of the above mechanisms to prevent self-sustained oscillations (of which the first is the more realistic) rely on providing stable steady states on the hysteresis loop of the AMOC nullcline. The more robust way in which to provide stability is to move the steady state away from the hysteresis loop entirely, and this is effected by varying F_*, which moves the black nullcline from side to side. It is clear that if F_* is too large or too small, there will be a single steady state on one or other of the stable branches of the ocean curve, as in figure 7 or 8. Again, under such parameters the system would tend towards this steady state.

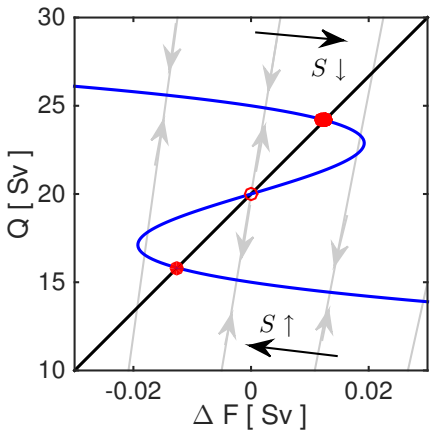

Figure 5. Alternative intersection of the nullclines when $\lambda = 0.003$, other parameters being as in figure 4. Both warm branch and cool branch steady states are stable, as shown by the red dots. Grey lines and arrows as described for figure 4.

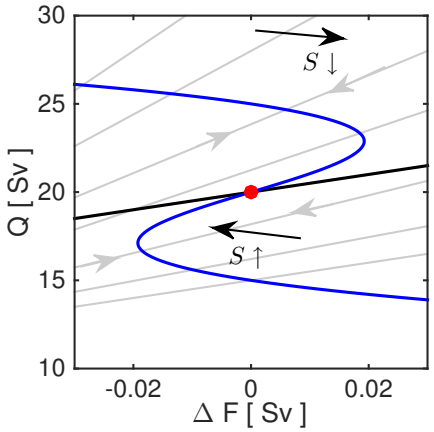

Figure 6. Equivalent phase plane to figure 4 but with smaller X. In this case, the steady state is rendered stable due to the decreased slopes of the grey lines, along which trajectories rapidly move back towards the blue AMOC nullcline. Importantly, the grey line passing through the steady state (red dot) has a shallower slope than the blue nullcline. Parameter values used here to illustrate this are as for figure 4, but with $X = 0.1$ Sv.

In summary therefore, for the system to exhibit self-sustained oscillations, the absolute value of $F_* = R_0 + R_N - E - F_0$ must not be too great, and λ must be sufficiently large (but not too much). Roughly speaking (the appendix details the conditions more precisely), this is the case if

$$|F_*| \ll b\Delta Q, \qquad b \lesssim \lambda \lesssim (X/R_0)\, b. \tag{13}$$

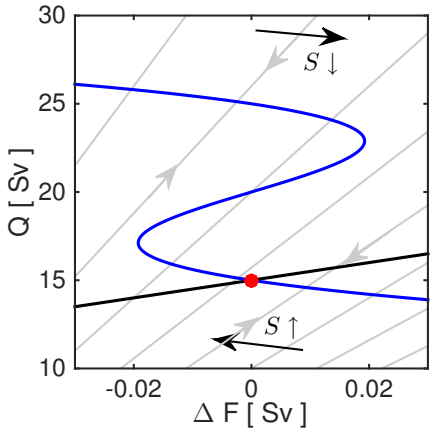

Figure 7. Stable cold branch solution for parameters as in figure 4, but with $F_* = 0.1$ Sv.

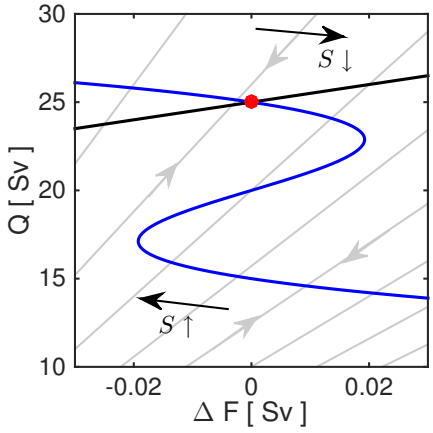

Figure 8. Stable warm branch solution for parameters as in figure 4, but with $F_* = -0.1$ Sv.

Excitable oscillations

Although we have concentrated on the interpretation of D-O cycles as self-sustained oscillations of a simple dynamical system, it is also possible to interpret the events as individual excursions of the system from an 'excitable' state, driven by some external perturbation (cf. *Peltier and Vettoretti* [2014]). This may, in fact, by a simpler way to account for much of the variability in the measured data.

Such an excitable mechanism is inherently built into our model, since the stable steady states on the upper and lower branches of the hysteresis curve in figures 7 and 8 are excitable in just this sense. A sudden external perturbation in freshwater forcing ΔF, can push the system over the edge of the stable branch and initiate a single excursion around the D-O trajectory. Such perturbations in F may be widely available, for instance, due to flooding from proglacial or subglacial lakes, to ice-berg discharge associated with Heinrich events (see below), or to sudden changes in the routing of meltwater runoff (the blockage and opening of the MacKenzie river route to the Arctic, for example).

Heinrich events deserve a further comment. It is important to note that they play no direct role in the mechanism for D-O events proposed here. Nevertheless, it is possible that they have some effect in modulating the cycles. It is presumed the Heinrich events represent a substantial drawdown of the Laurentide ice sheet, with corresponding massive discharge of ice-bergs across the North Atlantic [*MacAyeal*, 1993]. In our model, this would represent a sudden large increase in R_N and hence F_* (a consequent decrease in evaporation from the North Atlantic might further increase F_*). If the system is at that moment residing on the cold branch of the AMOC curve (see figure 4), this would have the effect of lengthening the cold period; in effect, the Heinrich event acts to negate the freshwater starvation that would otherwise be moving the system back towards the sudden warming. Indeed, there is evidence to suggest that cold stadials containing a Heinrich event tend to be long, and that the subsequent temperature rise is consequently large (see figure 1).

Variability

We now turn to a discussion of the variability of D-O events through the glacial period seen in figure 1. There are three principal features we wish to comment on. Firstly, D-O events are largely absent during marine isotope stages 2 and 4, when climate was cold, and in particular ice sheet volume was large. Secondly, D-O events do not occur in the present day climate, where there is no North American or Eurasian ice sheet providing runoff. And finally, the occurrence, duration and recurrence time of D-O events is distinctly variable. We attempt to interpret these observations in terms of our simple model.

The various possibilities for the dynamics are indicated in figures 4, 5, 7 and 8; we largely discount figure 6 on the basis that the parameter estimates suggest that it is unlikely to occur. As discussed above, the principal controls on these dynamics are the parameters λ and F_*. Since λ measures the sensitivity of Arctic runoff to changes in AMOC strength (via temperature), we anticipate that it may increase with the size of the ice sheets, since the area available for melting would increase, Thus, a sufficiently large ice sheet is required for this mechanism (though there is a caveat below concerning meltwater routing). In the current day, and in previous interglacials, λ is effectively zero, and there is no potential for D-O cycles as described here.

Another way in which λ might become very small is if the ice sheet margin advances sufficiently far south, such that most drainage occurs through the St Lawrence or Mississippi routes to the Atlantic, and not via the Mackenzie route to the Arctic [eg. *Clark et al.*, 2001]. The more southerly runoff would have little effect on AMOC. Thus, paradoxically, we envisage λ being lowest both for a small or non-existent ice sheet, and for a very large ice sheet.

The parameter F_* can be thought of as representing a background freshwater forcing. It includes net evaporation minus precipitation, as well as the magnitude of background runoff both into the Arctic and North Atlantic. It may be expected to vary through through the glacial period. While we associate colder climate with reduced evaporation, we also expect lower precipitation leading to a lower baseline runoff, and these competing effects make it hard to estimate the net effect on F_*. An increase in F_* would in principle cause transition from figure 8 through figure 4 to figure 7.

We now discuss the successive marine isotope stages in turn. Once the last interglacial (MIS 5e) is complete, the rest of MIS5 shows D-O activity but with long and highly variable periods. Two explanations appear possible in terms of our model. The first is that, while the ice sheet remains small, λ is low, and the system conforms to figure 5 or perhaps is close to the threshold between figure 5 and figure 4.

A small perturbation (such as a change in the background state, or a lake drainage event) can therefore tip it from the cold stable state to the warm one or vice versa. An alternative possibility is that climate sits in the stable but excitable state of figure 7 or figure 8.

As the climate cools further into MIS 4, one possibility is that lambda becomes small enough, because the large ice sheet favours the more southerly runoff routing, to become fixed on the cold branch in figure 5. An alternative is that changes in F^* are such that the S nullcline moves further to the right as in figure 7, and the cold branch becomes more stable. D-O events are not feasible, unless the ocean circulation is subjected to a large perturbation (which perhaps accounts for D-O 18).

In MIS3, climate is warmer and we suppose figure 4 or figure 5 is appropriate. In the former case, self-sustained oscillations could explain the cyclic D-O events, but another possibility is that the situation is akin to figure 5 or figure 7, where the climate is easily excitable. Following MIS3, the cold climate of MIS2 resumes the discussion of MIS4, and the final emergence of MIS1 after glacial termination moves the climate to the warm branch of figure 8, with small λ, when D-O events are no longer possible.

This qualitative discussion suggests a way of interpreting the ice core record in terms of a very simple model. The main quantitative feature of significance is the time scale of repetition, associated here with the period of the oscillation we predict. The solutions in figure 4 indicate a period of around 1,000 years, which is broadly consistent with the periods seen in figure 1. However, those periods are quite variable, and the event starting at ~ 104 ka lasts for ~ 14 ka. Two questions then arise: is our theory compatible with a period of 1,000 years? And is it able to deal with a variable period of as much as 10 ka?

From the analysis in appendix B we find that the period of oscillation in our model is given approximately by $(V/X)p$, where V is the Arctic Ocean volume, X is the Fram Strait exchange flux, and p is a dimensionless quantity which decreases weakly as λ/b increases, and increases as $|F_*|/b\Delta Q$ increases. The effect of both of these quantities on p turns out to be relatively weak (although becomes stronger as they approach the critical values at which the self-sustained oscillations disappear). Thus, the principal controller of the theoretical D-O period is the exchange flux X. To obtain a period of $\sim$ 1,000 y, we need (since $V \approx 600$ Sv y) $X \sim 0.6$ Sv, as compared with the present estimates of ~ 3 Sv. This provides a robust test for this theory: we require the exchange flux during glacial periods to be lower than present day estimates. That sea level was considerably lower makes this not an unreasonable possibility. However, the much longer period events would require even lower values of X, which seems unlikely. The more likely explanation for longer and more variable periods is that, as discussed previously, the system resides in a stable excitable state on the warm or cool branch, rather than a periodic oscillatory state. Slow migration of the steady state to the tipping point, through changes in λ or F_*, would then produce extended events, whose period is partly controlled by those external perturbations (and would therefore be more variable).

So it is not difficult in this theory to explain varying periods of the correct order, but it relies specifically on the Fram Strait exchange flux being lower than at present. It is a direct consequence of this that the Arctic salinity is markedly lower than at present. The model results in figure 4 suggest a salinity of about 30 ppt, and more generally, the analysis in appendix B shows that the Arctic salinity deficit (relative to the North Atlantic) is of the order of $\Delta S = S_N b\Delta Q/X$. This appears to be a significant test of the theory, and there is some evidence of Arctic salinity levels around this low value [*de Vernal et al.*, 2001], although the issue is clouded because much of the low salinity output from the Arctic occurs as a surface stream; our simple box model ignores the strong depth dependence of salinity.

The key feature allowing oscillations to occur is the ability for Arctic salinity to decrease significantly compared to the global ocean. In our model this is achieved if X is not too large. However it seems quite probable that the required isolation of Arctic water masses is more easily achieved when Bering Strait is closed. We therefore note that quasi-regular oscillations are observed in the ice-core record only after about 80 ka, which is a reasonable estimate for the closure date of Bering Strait [*Hu et al.*, 2012].

A further complicating aspect not mentioned in the discussion above is that the assumed hysteresis curve (blue line in figure 4 and following) has presumably itself changed throughout the glacial period, with changing sea level and surface forcings, and also due to the opening and closing of the Canadian Arctic Archipelago and Bering Strait. It is presumed that such change occurs on a longer timescale than the D-O cycles themselves, but it would provide another reason for variable timing and amplitude of the D-O events.

Comparison with other Salt Oscillators

It turns out that the model of *Birchfield and Broecker* [1990] is, in mathematical essence, very similar to that presented here, and a comparable mathematical framework is discussed in appendix C. The principal difference from our work is that in that model, the buffering volume for salinity change is the Atlantic itself; and the assumed AMOC hysteresis is dependent on this mean Atlantic salinity, rather than on the freshwater forcing F.

The salinity in that model is controlled by AMOC-dependent runoff from the ice sheets, as well as by exchange with the world ocean, partly driven by AMOC in tandem with the Antarctic circumpolar current (ACC). The period of oscillations scales as V_a/Q_0, where $V_a \approx 3.1 \times 10^{17}$ m^3 is the volume of the Atlantic, and $Q_0 \sim 30$ Sv is the exchange flux with the world ocean. This is analogous to the time scale V/X in the present model. In essence, the Pacific, the ACC and the Atlantic take the rôles of the North Atlantic, Fram Strait flux and the Arctic in the present model.

One key advantage of our model is that it takes account of freshwater routing to the North Atlantic, and allows for a more coherent discussion of the effects of differently sized ice sheets on meltwater runoff rates, and the consequent variability in duration and recurrence time which may ensue.

Peltier and Vettoretti [2014] invoke the idea of an excitable salt oscillator to explain the behaviour of their general circulation model. The resulting relaxation oscillations bear considerable resemblance to those in our simple model, but the mechanism appears to be slightly different. Variable run-off from the ice sheet is specifically excluded from that model, and the oscillations have a purely oceanographic origin.

4. Conclusions

We have constructed a simple model to explain how D-O cycles could have occurred in a self-sustained manner during the glacial period. The mechanism is extremely simple. It essentially lies in the fact that there is more runoff from the ice sheets during the warm interstadial periods than the cold stadials. Of course, we also rely heavily on the assumed ocean hysteresis that responds to this runoff, and that is a common underpinning of many previous explanations too. There is ongoing debate about the true controls on

AMOC; the manner in which local buoyancy forcing drives deep water formation, whether bistability or multiple equilibria manifest themselves in eddy-resolving models, and the extent to which the precise location and timing of freshwater inputs are important [*e.g. Weijer et al., 2012; den Toom et al., 2014]*. A specific motivation for our study was the observation that deep water formation appears to be particularly sensitive to Arctic-derived water [*Rennermalm et al.*, 2006; *Condron and Winsor*, 2012].

A key rôle is also played by the variations in runoff from the ice sheets, which have been assumed to depend on the mean northern hemisphere temperature, with slower modifications due to the growth and shrinkage of the ice sheets. Other factors affecting freshwater forcing have been crudely rolled into the parameters F_* and λ, and this is almost certainly a gross simplification. It is likely that the glacial period, and perhaps the individual D-O cycles themselves, saw significant changes in evaporation and precipitation patterns, sea ice production and export, and smaller scale adjustments in ocean circulation. A more detailed inclusion of these effects in our model would certainly be worthwhile. Indeed, an obvious next step in testing these ideas is to use a general circulation model, in which the hysteretic behaviour of the ocean is derived rather than simply imposed.

This provides further incentive for the full coupling of ice-sheet dynamics in such models, which would enable the growth and decay of the ice sheets, and consequent changes in runoff, to be fully explored. Given the sensitivity of ocean models to the specific locations of freshwater forcing, there is an interesting competition between increased sensitivity of runoff to temperature as the ice sheets grow and the potentially significant re-routing of meltwater as the margins advance and retreat [*Clark et al.*, 2001; *Gowan*, 2013].

As well as more detailed modelling, improved parameter estimates and other proxy evidence could help test whether the mechanism suggested here is important. Specific implications of the model are that the Fram Strait exchange flow should have been reduced from its current level, that the mean Arctic salinity was also lower than the present day, and that this salinity slowly varied through the D-O cycles (a similar pattern of salinity change was inferred for the Norwegian Sea by *Dokken et al.* [2013]).

It is worthwhile to emphasise that many of the mechanisms previously suggested for D-O events are not necessarily inconsistent with the ideas presented here. Indeed, changes in the sea-ice edge [e.g. *Li et al.*, 2005] and in atmospheric circulation [e.g. *Zhang et al.*, 2014], may be needed to generate our assumed response of temperature and hence runoff to AMOC. However, the appeal of this mechanism is that the self-sustained oscillations arise as a natural dynamical consequence of the ice-age water cycle. The identification of a relaxation oscillation provides a reason for the surprising regularity of the period between many of the warming events [*Rahmstorf*, 2003], while any of the complications discussed above are likely to cause variability. The fact that the same system can become stable during periods of low ice volume, or during particularly cold periods, suggests a reason for the absence of D-O events during interglacials and around the glacial maxima.

Appendix A: Effective freshwater flux

When freshwater is delivered directly to the North Atlantic, the meaning of the freshwater flux is clear. However, when freshwater is delivered to the Arctic, causing a saline inflow to the North Atlantic, it is less obvious how the effective freshwater flux should be defined. To answer this question, imagine first that there is no separate Arctic Ocean, and that the North Atlantic receives a direct freshwater flux F, and there is no evaporation. There is then a compensating flux F to the south, and salt conservation for the North Atlantic would imply

$$V_N \frac{dS_N}{dt} = -FS_N, \tag{A1}$$

This can be used to define the freshwater flux more generally as

$$F = -\frac{V_N}{S_N}\frac{dS_N}{dt}. \tag{A2}$$

(These two expressions ignore the large exchange of saline water with the rest of the Atlantic, due to the AMOC, which actually has the effect of maintaining S_N at a relatively constant value. The dS_N/dt term here represents the rate of change that *would* occur if the extra input F were the only influence on North Atlantic salinity.)

Now consider the system in figure 3. We first write down a salt conservation equation for the the Arctic Ocean, which is simply

$$V\frac{dS}{dt} = X(S_N - S) - R_A S. \tag{A3}$$

The right hand side is the net flux of salt into the Arctic. The influence of this flux on the North Atlantic salt balance is therefore

$$V_N \frac{dS_N}{dt} = -X(S_N - S) + R_A S - (R_A + R_N - E)S_N, \tag{A4}$$

(the final term here is again the volume-compensating flow to the south), and it follows from (A2) that the freshwater flux is

$$F = R_N - E + \frac{(X + R_A)(S_N - S)}{S_N}. \tag{A5}$$

In the absence of the exchange flow X through the Fram Strait, and if the Arctic were a freshwater lake, $S = 0$, we see that this expression reduces to the expected value $F = R_N + R_A - E$.

We write F in terms of its difference from the reference value F_0 as

$$\Delta F \equiv F - F_0 = \frac{(X + R_A)(S_N - S)}{S_N} - R_0 + F_*, \tag{A6}$$

with

$$F_* = R_0 + R_N - E - F_0. \tag{A7}$$

The equation $R_A(Q)$ from (7) can be substituted into (A6) to arrive at the expression given in (8).

Appendix B: Analysis of the model

We analyse the pair of equations (10) and (11), with the functions ΔF and Φ defined by (8) and (2), respectively. First we scale the variables by taking

$$Q = Q_0 + \Delta Q\, q, \quad \Phi = b\Delta Q\, \phi, \quad \Delta F = b\Delta Q\, f,$$

$$S_N - S = \Delta S\, s, \quad \Delta S = \frac{S_N b \Delta Q}{X}, \quad t \sim t_0 = \frac{V}{X}, \tag{B1}$$

so that the dimensionless equations become

$$\varepsilon \dot{q} = \phi - f, \qquad \dot{s} = \rho_* + \Lambda q - f, \tag{B2}$$

where

$$f(q, s) = s(1 + \beta\rho_0 + \beta\Lambda q) - \rho_0 + \rho_*,$$
$$\phi(q) = q(1 - q^2), \tag{B3}$$

and the dimensionless parameters are

$$\rho_* = \frac{F_*}{b\Delta Q}, \quad \rho_0 = \frac{R_0}{b\Delta Q}, \quad \varepsilon = \frac{\tau}{t_0} = \frac{\tau X}{V},$$

$$\beta = \frac{b\Delta Q}{X}, \quad \Lambda = \frac{\lambda}{b}, \tag{B4}$$

where F_* was defined in (9). (Note the dimensionless variable f used here is different from the function $f(Q)$ in (4), which was replaced by (1) and used no further).

Using our estimates $V = 1.9 \times 10^{16}$ m^3 $\approx$ 600 Sv y, $S_N = 36$ ppt, $X = 3$ Sv, $\lambda = 0.01$, $F^* \ll R_0 \sim 0.1$ Sv, $\tau \sim 10$ y, $b \sim 0.01$, $Q_0 \sim 20$ Sv, $\Delta Q \sim 5$ Sv, we find

$$\rho_* \ll 1, \quad \rho_0 \sim 2, \quad \varepsilon \sim 0.05, \quad \beta \sim 0.017, \quad \Lambda \sim 1. \tag{B5}$$

On the basis that $\varepsilon \ll 1$, q rapidly approaches the quasi-equilibrium 'slow manifold' on which, since $\beta \ll 1$,

$$f \approx s - \rho_0 + \rho_* \approx q(1 - q^2). \tag{B6}$$

The evolution of s on the slow manifold is then given by

$$\dot{s} = \rho_* + \Lambda q - f \approx \rho_0 + \Lambda q - s. \tag{B7}$$

The conditions for oscillations are mostly controlled by the intersections of the two nullclines $f = \Lambda q + \rho_*$ (for s) and $f = q(1 - q^2)$ (for q). These intersections determine the steady states of the system, of which there are either one, two (exceptionally), or three. Self-sustaining oscillations occur if all of these steady states are unstable, which, since $\varepsilon \ll 1$, requires that they all lie on the central unstable branch of the hysteresis curve. This will occur provided the inverse slope of the s null-cline (the black line in figure 4) is sufficiently large, specifically if $\Lambda > 2/3 + |\rho_*|/\sqrt{3}$. (The typical situation, as in figure 4, is for only a single steady state, which occurs if $\Lambda > 1 - 3|\rho_*|^{2/3}/2^{2/3}$, but it is also possible to have three steady states all on the central branch.) Clearly there are two primary ways in which to lose the self-sustaining oscillations; either Λ becomes too small (this is the case in figure 5), or $|\rho_*|$ becomes too large (this is the case in figures 7 and 8).

However, it is also possible for the steady states on the central branch to become stable if Λ is too large, in which case the small β approximation made in (B6) becomes invalid. In fact, this condition underlies the loss of cyclicity shown in figure 6. The rapid approach to the quasi-equilibrium $f = \phi(q)$ occurs with s constant, and in the f–q phase plane, which is the dimensionless version of the ΔF–Q phase plane of figure 6, this occurs along lines (the grey lines in the figures) with inverse slope $\partial f/\partial q = \beta\Lambda s$ (from (B3)). The steady state becomes stable if this inverse slope is greater than the slope of $\phi(q)$ at that point. This is the case in figure 6, where the steady state at $q = 0$ has $s \approx \rho_0$, and therefore becomes stable if $\beta\Lambda\rho_0 \gtrsim 1$. Since also we suppose $\Lambda \sim 1$, the approximate criterion for this stability (and hence loss of self-sustained oscillations) is just $\beta\rho_0 \gtrsim 1$, or equivalently $X \lesssim R_A$. We consider this to be a very unlikely situation.

Assuming periodic solutions exist, their period can be estimated as the time taken to traverse the upper and lower branches of the slow manifold, from $q = \pm 2/\sqrt{3}$ to $q = \pm 1/\sqrt{3}$. This is

$$p = \int dt = \int \frac{ds}{\dot{s}} \approx \int_{1/\sqrt{3}}^{2/\sqrt{3}} \frac{(3q^2 - 1)\, dq}{q(\Lambda - 1 + q^2) + \rho_*} + \int_{1/\sqrt{3}}^{2/\sqrt{3}} \frac{(3q^2 - 1)\, dq}{q(\Lambda - 1 + q^2) - \rho_*}, \tag{B8}$$

(using the approximations $\varepsilon \ll 1$ and $\beta \ll 1$). For the particular value $\rho_* = 0$, corresponding to figure 4, this is

$$p = \frac{1}{\Lambda - 1}\left[(3\Lambda - 2)\ln\left(\frac{\Lambda + \frac{1}{3}}{\Lambda - \frac{2}{3}}\right) - 2\ln 2\right]; \tag{B9}$$

this is an $O(1)$ monotonically decreasing function of Λ with a maximum of $\ln 64 \approx 4.16$ when $\Lambda = \frac{2}{3}$.

Perhaps of more interest is the dependence on ρ_*. The formula given by (B8) is a monotonically increasing function of $|\rho_*|$; although this tends to a finite value as $\rho_* \to \pm\left(\Lambda - \frac{2}{3}\right)/\sqrt{3}$, when the intersection point of the two null-clines reaches one or other turning point of the hysteresis curve, the relaxation-oscillation approximation breaks down there, and in fact the period must tend to infinity.

Appendix C: The Birchfield–Broecker model

Birchfield and Broecker [1990] present a model which is very similar to that presented here, except that the buffering ocean is the Atlantic itself. We provide a brief mathematical formulation of their model in a comparable format to our own, to help illustrate the similarities and differences.

By analogy with figure 3, the model can be rationalised in terms of the compartment diagram shown in figure 10. Their equation for Atlantic salinity (which can be compared with our (A3)), can be written

$$V_a \frac{dS_a}{dt} = mS_p + Q(S_p - S_a), \tag{C1}$$

where V_a and S_a are the volume and mean salinity of the Atlantic, S_p the mean Pacific salinity, Q the exchange flux between the two, and m the net freshwater flux to the Atlantic, defined further below (*Birchfield and Broecker* [1990] wrote mS_0 instead of mS_p, but the difference is illusory; simply rescale m).

Freshwater flows into, and is evaporated from, the Atlantic, which also exchanges salinity with the rest of the world Ocean (essentially the Pacific), through the agency of the Antarctic circum-polar current. The exchange flux Q is given by the hysteretic prescription

$$\begin{aligned} Q &= Q_m \equiv A, \quad S < S_M, \\ Q &= Q_M \equiv A + m_0, \quad S > S_m, \end{aligned} \tag{C2}$$

where $S_m < S_M$ are threshold values, A represents a mixing rate with the world ocean, and m_0 is the AMOC when

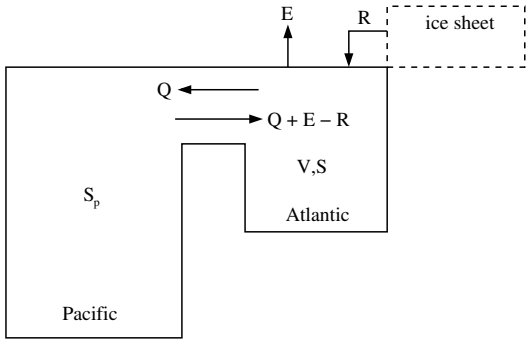

Figure 10. A schematic box model, analogous to figure 3, consistent with the derivation of the *Birchfield and Broecker* [1990] model. The runoff R is taken to be negative when the ice sheet is growing.

this circulation is on (we adopt the notation from *Birchfield and Broecker* [1990]). Analogously to our procedure in the current paper, this hysteretic recipe can be rationalised by defining the evolution equation for Q,

$$\frac{\tau \Delta S}{\Delta Q}\frac{dQ}{dt} = S - g(Q), \tag{C3}$$

where $g(Q)$ is a non-monotonic equilibrium function as indicated in figure 9. Specifically, we define

$$\Delta S = S_M - S_0, \quad \Delta Q = Q_M - Q_0,$$
$$S_0 = \tfrac{1}{2}(S_M + S_m), \quad Q_0 = \tfrac{1}{2}(Q_M + Q_m), \tag{C4}$$

and take

$$g(Q) = S_0 + \Delta S\, \psi(q), \qquad Q = Q_0 + \Delta Q\, q, \tag{C5}$$

with

$$\begin{aligned} &\psi = -q, \quad |q| < 1, \\ &\psi < 1, \quad q = -1, \\ &\psi > -1, \quad q = 1. \end{aligned} \tag{C6}$$

The evolution equation (C3) ensures that Q rapidly approaches one of the quasi-steady states Q_m or Q_M, on a rapid time scale τ.

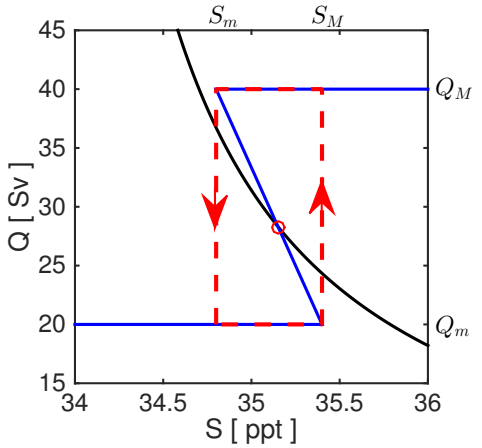

Figure 9. Phase plane for the salt oscillator described by (C1)-(C3). The blue curve shows the function $S = g(Q)$, which is the assumed equilibrium to which Q rapidly approaches according to (C3), and the black curve is the S-nullcline, which is the equilibrium of (C1). For the parameters chosen, as given in the text, oscillations occur as indicated by the red trajectory.

Birchfield and Broecker [1990] take the net export of freshwater from the Atlantic to be $m = E - R$ when $Q = Q_M$, i. e., when the AMOC is on; here $E = m_p$ is evaporation rate and $R = m_i$ is the runoff from the ice sheet; on the other hand when the AMOC is off, $Q = Q_m$ and Birchfield and Broecker take $m = m_p + m_i$, assuming that ice sheet growth takes place at a rate which is just the negative of the melt rate. Both of these prescriptions are consistent with a choice of m dependent on Q as

$$m = m_p - \frac{m_i}{\Delta Q}(Q - Q_0), \tag{C7}$$

which we assume. This prescription is analogous to our assumed dependence of R_A on Q in appendix B.

We analyse the model (C1) and (C3) together with the function prescriptions (C7) for $m(Q)$, and (C5) for $g(Q)$. We proceed as in appendix B. We non-dimensionalise the variables by writing

$$S = S_0 + \Delta S\, s, \quad Q = Q_0 + \Delta Q\, q, \quad t \sim t_0 = \frac{V_a}{Q_0}, \tag{C8}$$

and this leads to the dimensionless system

$$\begin{aligned} \varepsilon \dot{q} &= s - \psi(q), \\ \dot{s} &= \mu(1 - \alpha q) - (1 + \delta q)(s + \rho), \end{aligned} \tag{C9}$$

where the parameters are defined by

$$\alpha = \frac{m_i}{m_p}, \quad \delta = \frac{\Delta Q}{Q_0}, \quad \varepsilon = \frac{\tau Q_0}{V_a},$$
$$\mu = \frac{S_p m_p}{Q_0 \Delta S}, \quad \rho = \frac{S_0 - S_p}{\Delta S}. \tag{C10}$$

Using the values of *Broecker et al.* [1990], $\Delta S = 0.3$ ppt, $S_0 = 35.1$ ppt, $Q_0 = 30$ Sv, $\Delta Q = 10$ Sv, $V_a = 3.1 \times 10^{17}$ m^3, $S_p = 34.66$ ppt, $m_i = 0.1$–0.3 Sv, but we choose 0.3 Sv to be specific, $m_p = 0.35$ Sv, $\tau = 10$ y, we find typical values of the dimensionless parameters to be

$$\alpha \sim 0.86, \quad \delta \sim 0.33, \quad \varepsilon \sim 0.03, \quad \mu \sim 1.35, \quad \rho \sim 1.4; \tag{C11}$$

the time scale is $t_0 \sim 328$ y.

Just as in appendix B, q relaxes rapidly to a quasi-equilibrium $s = \psi(q)$ (corresponding to the blue curve in figure 9), following which s more slowly relaxes towards the s-nullcline

$$s = N(q) \equiv \frac{\mu(1 - \alpha q)}{1 + \delta q} - \rho, \tag{C12}$$

which corresponds to the black curve in figure 9. The s-nullcline gives s as a decreasing function of q, and thus also q as a decreasing function of s. The issue of whether oscillations occur depends on the intersections of the two nullclines. It is clear from figure 9 (which simply represents the dimensional version of the graphs of $s = \psi(q)$ and the s-nullcline $s = N(q)$ in (C12)) that oscillations will occur if $N(1) < -1$ and $N(-1) > 1$ (since $\psi(\pm 1) = \mp 1$). Using (C12), these conditions can be written after some algebra in terms of m_i and m_p as

$$\begin{aligned} m_p - m_i &< \frac{Q_M(S_m - S_p)}{S_p} \approx 0.16, \\ m_p + m_i &> \frac{Q_m(S_M - S_p)}{S_p} \approx 0.43, \end{aligned} \tag{C13}$$

where the numerical values are for the default values of the constants, as given above. This gives the instability region as a quadrant in the (m_i, m_p) plane, as shown by *Birchfield and Broecker* [1990] (their figure 3); the reason the period of the oscillation becomes infinite at the boundaries of these regions is because the intersection point (steady state) of the two nullclines tends to one or other of the corner points in figure 9 (in dynamical systems terminology, this is a blue sky catastrophe, where a limit cycle collides with a fixed point).

Of the parameters suggested by *Birchfield and Broecker* [1990], only the runoff rate m_i is given a range, from 0.1 to 0.3 Sv. If m_i is lowered from 0.3 to 0.1, the black curve in figure 9 moves upwards, so the period first lengthens, and then the periodic solution disappears, with a stable steady state emerging on the upper, warm branch. The opposite behaviour occurs if the black curve moves the other way.

Acknowledgments.
This paper is the outcome of two workshops held in July and September 2013, funded by grants from the Oxford Centre for Collaborative Applied Mathematics and Corpus Christi College, Oxford, and by a Philip Leverhulme Prize awarded to C.R.S. I. J. H. is supported by a Marie Curie Career Integration Grant. E. W. W. is funded by a Royal Society Research Professorship. A. C. F. acknowledges the support of the Mathematics Applications Consortium for Science and Industry (`www.macsi.ul.ie`) funded by the Science Foundation Ireland grant 12/1A/1683.

References

Aagard, K., and E. C. Carmack (1989), The role of sea ice and other fresh water in the arctic circulation, *J. Geophys. Res.*, *94*, 14,485–14,498.

Barker, S., G. Knorr, R. L. Edwards, F. Parrenin, A. E. Putnam, L. C. Skinner, E. W. Wolff, and M. Ziegler (2011), 800,000 years of abrupt climate variability, *Science*, *334*(6054), 347–351.

Birchfield, G. E., and W. S. Broecker (1990), A salt oscillator in the glacial atlantic? 2. a "scale analysis" model, *Paleoceanography*, *5*, 835–843.

Blunier, T., and E. J. Brook (2001), Timing of millennial-scale climate change in Antarctica and Greenland during the last glacial period, *Science*, *291*(5501), 109–112.

Bond, G., H. Heinrich, W. Broecker, L. Labeyrie, J. McManus, J. Andrews, S. Huon, R. Jantschik, S. Clasen, C. Simet, K. Tedesco, M. Klas, G. Bonani, and S. Ivy (1992), Evidence for massive discharges of icebergs into the north atlantic ocean during the last glacial period, *Nature*, *360*, 245–249.

Bretz, J. H. (1923), The channeled scablands of the columbia plateau, *J. Geol.*, *31*, 617–649.

Broecker, W. S., M. Andree, W. Wolffi, H. Oeschger, G. Bonani, J. Kennett, and D. Peteet (1988), The chronology of the last deglaciation: implications to the cause of the younger dryas event, *Paleoceanography*, *3*, 1–19.

Broecker, W. S., G. Bond, M. Klas, G. Bonani, and W. Wolffi (1990), A salt oscillator in the glacial atlantic? 1. the concept, *Paleoceanography*, *5*, 469–477.

Carlson, A. E., and P. U. Clark (2012), Ice sheet sources of sea level rise and freshwater discharge during the last deglaciation, *Rev. Geophys.*, *50*, RG4007.

Clark, P. U., S. J. Marshall, G. K. C. Clarke, S. W. Hostetler, J. M. Licciardi, and J. T. Teller (2001), Freshwater forcing of abrupt climate change during the last glaciation, *Science*, *293*, 283–287.

Clarke, G. K. C., D. W. Leverington, J. T. Teller, and A. S. Dyke (2004), Paleohydraulics of the last outburst flood from glacial lake agassiz and the 8200 bp cold event, *Quat. Sci. Revs.*, *23*, 389–407.

Condron, A., and P. Winsor (2012), Meltwater routing and the Younger Dryas, *PNAS*, *109*, 19,928–19,933.

Dansgaard, W., S. Johnsen, H. Clausen, D. Dahl-Jensen, N. Gundestrup, C. Hammer, C. Hvidberg, J. Steffensen, A. Sveinbjornsdottir, J. J., and G. Bond (1993), Evidence for general instability of past climate from a 250 kyr ice-core record, *Nature*, *264*, 218–220, doi:10.1038/364218a0.

de Vernal, A., M. Henry, J. Matthiessen, P. J. Mudie, A. Rochon, K. P. Boessenkool, F. Eynaud, K. Grøsfjeld, J. Guiot, D. Hamel, R. Harland, M. J. Head, M. Kunz-Pirrung, E. Levac, V. Loucheur, O. Peyron, V. Pospelova, T. Radi, J.-L. Turon, and E. Voronina (2001), Dinoflagellate cyst assemblages as tracers of sea-surface conditions in the northern north atlantic, arctic and sub-arctic seas: the new 'n = 677' data base and its application for quantitative palaeoceanographic reconstruction, *J. Quat. Sci.*, *16*, 681–698.

den Toom, M., H. A. Dijkstra, W. Weijer, M. W. Hecht, M. E. Maltrud, and E. van Sebille (2014), Response of a strongly eddying global ocean to north atlantic freshwater perturbations, *J. Phys. Oceanography*, *44*, 464–481.

Denton, G. H., R. B. Alley, G. C. Comer, and W. S. Broecker (2005), The role of seasonality in abrupt climate change, *Quat. Sci. Revs.*, *24*, 1159–1182.

Dokken, T. M., K. H. Nisancioglu, C. Li, D. S. Battisti, and C. Kissel (2013), Dansgaard–oeschger cycles: interactions between ocean and sea ice intrinsic to the nordic seas, *Paleoceanography*, *28*, 491–502.

Eakins, B. W., and G. F. Sharman (2010), Volumes of the World's Oceans from ETOPO1, *NOAA National Geophysical Data Center, Boulder, CO*.

EPICA Community Members (2006), One-to-one hemispheric coupling of millennial polar climate variability during the last glacial, *Nature*, *444*, 195–198.

Fahrbach, E., J. Meincke, S. Østerhus, G. Rohardt, U. Schauer, V. Tverberg, and J. Verduin (2001), Direct measurements of volume transports through fram strait, *Polar Research*, *20*, 217–224.

Fricker, H. A., and T. Scambos (2009), Connected subglacial lake activity on lower mercer and whillans ice streams, west antarctica, 2003–2008, *J. Glaciol.*, *55*, 303–315.

Ganopolski, A., and S. Rahmstorf (2001), Rapid changes of glacial climate simulated in a coupled climate model, *Nature*, *409*, 153–158.

Gildor, H., and E. Tziperman (2003), Sea-ice switches and abrupt climate change, *Phil. Trans. R. Soc. Lond. A*, *361*, 1935–1944.

Gowan, E. J. (2013), An assessment of the minimum timing of ice free conditions of the western Laurentide Ice Sheet, *Quaternary Science Reviews*, *75*, 100–113.

Hawkins, E., R. S. Smith, L. C. Allison, J. M. Gregory, T. J. Woollings, H. Pohlmann, and B. de Cuevas (2011), Bistability of the Atlantic overturning circulation in a global climate model and links to ocean freshwater transport, *Geophys. Res. Lett.*, *38*, L10,605, doi:10.1029/2011GL047208.

Heinrich, H. (1988), Origin and consequences of cyclic ice rafting in the northeast north atlantic ocean during the past 130,000 years, *Quat. Res.*, *29*, 142–152.

Hemming, S. R. (2004), Heinrich events: Massive late pleistocene detritus layers of the North Atlantic and their global climate imprint, *Revs. Geophys.*, *42*, RG1005.

Hu, A., et al. (2012), Role of the Bering Strait on the hysteresis of the ocean conveyor belt circulation and glacial climate stability, *PNAS*, *109*, 6417–6422.

Johnsen, S. J., H. B. Clausen, W. Dansgaard, K. Fuhrer, N. Gundestrup, C. U. Hammer, P. Iversen, J. Jouzel, B. Stauffer, and J. P. Steffensen (1992), Irregular glacial interstadials recorded in a new Greenland ice core, *Nature*, *359*, 311–313.

Johnson, H., D. P. Marshall, and D. A. J. Sproson (2007), Reconciling theories of a mechanically driven meridional overturning circulation with thermohaline forcing and multiple equilibria, *Clim. Dyn.*, doi:10.1007/s00382-007-0262-9.

Jouzel, J., et al. (2007), Orbital and millennial antarctic climate variability over the last 800,000 years, *Science*, *317*, 793–796.

Kageyama, M., et al. (2013), Climatic impacts of fresh water hosing under last glacial maximum conditions: a multi-model study, *Clim. Past*, *9*, 935–953.

Li, C., D. S. Battisti, D. P. Schrag, and E. Tziperman (2005), Abrupt climate shifts in greenland due to displacements of the sea ice edge, *Geophys. Res. Lett.*, *32*, L19,702.

MacAyeal, D. R. (1993), Binge/purge oscillations of the laurentide ice sheet as a cause of the north atlantic's heinrich events., *Paleoceanography*, *8*, 775–784.

Menviel, L., A. Timmermann, T. Friedrich, and M. H. England (2014), Hindcasting the continuum of Dansgaard–Oeschger variability: mechanisms, patterns and timing, *Clim. Past*, *10*, 63–77.

North Greenland Ice Core Project Members (2004), High-resolution record of northern hemisphere climate extending into the last interglacial period, *Nature*, *431*, 147–151.

Peltier, W. R., and G. Vettoretti (2014), Dansgaard-oeschger oscillations predicted in a comprehensive model of glacial climate: A "kicked" salt oscillator in the atlantic, *Geophys. Res. Letts.*, *41*, 7306–7313.

Petersen, S. V., D. P. Schrag, and P. U. Clark (2013), A new mechanism for dansgaard–oeschger cycles, *Paleoceanography*, *28*, 24–30.

Peterson, L. C., G. H. Haug, K. A. Hughen, and U. Rohl (2000), Rapid changes in the hydrologic cycle of the tropical Atlantic during the last glacial, *Science*, *290*, 1947–1951.

Rahmstorf, S. (1995), Bifurcations of the Atlantic thermohaline circulation in response to changes in the hydrological cycle, *Nature*, *378*, 145–149.

Rahmstorf, S. (2003), Timing of abrupt climate change: A precise clock, *Geophys. Res. Lett.*, *30*, 1510.

Rahmstorf, S., et al. (2005), Thermohaline circulation hysteresis: A model intercomparison, *Geophys. Res. Lett.*, *32*, doi:10.1029/2005GL023655.

Rennermalm, A., E. Wood, S. Dery, A. Weaver, and M. Eby (2006), Sensitivity of the thermohaline circulation to arctic ocean runoff, *Geophys. Res. Lett.*, *33*(L12703), doi: 10.1029/2006GL026124.

Shackleton, N. J., M. A. Hall, and E. Vincent (2000), Phase relationships between millennial-scale events 64,000-24,000 years ago, *Paleocenaography*, *15*, 565–569.

Stocker, T. F., and S. J. Johnsen (2003), A minimum thermodynamic model for the bipolar seesaw, *Paleoceanography*, *18*, 1087.

Stommel, H. (1961), Thermohaline convection with two stable regimes of flow, *Tellus XIII*, *2*, 224–230.

Tarasov, L., and R. Peltier (2005), Arctic freshwater forcing of the Younger Dryas cold reversal, *Nature*, *435*, 662–665.

Wang, Y. J., H. Cheng, R. L. Edwards, Z. S. An, J. Y. Wu, C. C. Shen, and J. A. Dorale (2001), A high-resolution absolute-dated late pleistocene monsoon record from Hulu Cave, China, *Science*, *294*, 234–2348.

Wang, Z., and L. A. Mysak (2006), Glacial abrupt climate changes and dansgaard-oeschger oscillations in a coupled climate model, *Paleoceanography*, *21*, PA2001.

Weijer, W., M. E. Maltrud, M. W. Hecht, H. A. Dijkstra, and M. A. Kliphuis (2012), Response of the Atlantic Ocean circulation to Greenland Ice Sheet melting in a strongly-eddying ocean model, *Geophys. Res. Lett.*, *39*, L09,606, doi:10.1029/2012GL051611.

Wingham, D. J., M. J. Siegert, A. Shepherd, and A. S. Muir (2006), Rapid discharge connects antarctic subglacial lakes, *Nature*, *440*, 1,033–1,037.

Wolff, E. W., J. Chappellaz, T. Blunier, S. O. Rasmussen, and A. Svensson (2010), Millennial-scale variability during the last glacial: the ice core record, *Quat. Sci. Rev.*, *29*, 2828–2838.

Zhang, X., G. Lohmann, G. Knorr, and C. Purcell (2014), Abrupt glacial climate shifts controlled by ice sheet changes, *Nature*, *512*, 290–294.

Corresponding author: Ian Hewitt, Mathematical Institute, University of Oxford, OX2 6GG (hewitt@maths.ox.ac.uk)